Applied Microbiology and Biotechnology (2024) 108:478
https://doi.org/10.1007/s00253-024-13304-1

BIOTECHNOLOGICALLY RELEVANT ENZYMES AND PROTEINS

Random mutagenesis and disulfide bond formation improved thermostability in microbial transglutaminase

Mototaka Suzuki[1] · Masayo Date[1] · Tatsuki Kashiwagi[1] · Kazutoshi Takahashi[1] · Akira Nakamura[2] · Masaru Tanokura[2] · Eiichiro Suzuki[1,3] · Keiichi Yokoyama[1,4]

Received: 2 July 2024 / Revised: 30 August 2024 / Accepted: 3 September 2024

Abstract

Microbial transglutaminase (MTG) from *Streptomyces mobaraensis* is widely used in the food and pharmaceutical industries for cross-linking and post-translational modification of proteins. It is believed that its industrial applications could be further broadened by improving its thermostability. In our previous study, we showed that the introduction of structure-based disulfide bonds improved the thermostability of MTG, and we succeeded in obtaining a thermostable mutant, D3C/G283C, with a T_{50} (incubation temperature at which 50% of the initial activity remains) 9 °C higher than that of wild-type MTG. In this study, we performed random mutations using D3C/G283C as a template and found several amino acid substitutions that contributed to the improvement of thermostability, and investigated a thermostable mutant (D3C/S101P/G157S/G250R/G283C) with three amino acid mutations in addition to the disulfide bond. The T_{50} of this mutant was 10 °C higher than that of the wild type, the optimal temperature for enzymatic reaction was increased to 65 °C compared to 50 °C for the wild type, and the catalytic efficiency (k_{cat}/K_m) at 37.0 °C was increased from 3.3×10^2 M^{-1} s^{-1} for the wild type to 5.9×10^2 M^{-1} s^{-1}. X-ray crystallography of the D3C/G283C MTG showed no major structural differences against wild-type MTG. Structural differences were found that may contribute to thermostabilization and improve catalytic efficiency.

Key points

- *Improved heat resistance is essential to broaden the application of MTG.*
- *The MTG mutant D3C/S101P/G157S/G250R/G283C showed improved thermostability.*
- *X-ray crystallography of the disulfide bridge mutant D3C/G283C MTG was elucidated.*

Keywords Microbial transglutaminase · Heat resistance · Disulfide bridge · Random mutation · X-ray crystallography

Introduction

Transglutaminases (TGases: protein-glutamine γ-glutamyltransferases, EC 2.3.2.13) catalyze the transfer of an acyl group between the γ-carboxyamide group of the glutamine residue and the ε-amino group of the lysine residue in a peptide, resulting in the formation of an ε-(γ-glutamyl) lysine bridge (Ikura et al. 1988). TGases are widely distributed in various mammalian cells and tissues and their physiological properties have been previously studied (Folk 1980).

Streptomyces mobaraensis TGase (MTG; microbial transglutaminase), unlike TGases from mammals, has been characterized by its calcium-independent activity (Ando et al. 1989) (Nonaka et al. 1989), and its three-dimensional structure has been analyzed by crystallization and revealed to be a protein with a single, compact domain (Kashiwagi

✉ Keiichi Yokoyama
keiichia.yokoyama.d7e@asv.ajinomoto.com

Tatsuki Kashiwagi
kashiwagi.tatsuki@cocoa.plala.or.jp

[1] Institute for Innovation, Ajinomoto Co., Inc., 1-1, Suzuki-Cho, Kawasaki-Shi, Kanagawa 210-8681, Japan

[2] Department of Applied Biological Chemistry, Graduate School of Agricultural and Life Sciences, The University of Tokyo, 1-1-1 Yayoi, Bunkyo-Ku, Tokyo 113-8657, Japan

[3] Present Address: Kihara Memorial Yokohama Foundation for the Advancement of Life Sciences Yokohama Bio Industry Center, 1-6 Suehiro-Cho, Yokohama, Tsurumi-Ku 230-0045, Japan

[4] Present Address: R&B Planning Department, Ajinomoto Co., Inc., Tokyo 104-8315, Japan

Published online: 01 October 2024

et al. 2002). For previous studies on MTG, see the review by Fuchsbauer (2021).

MTG is expressed as pro-MTG, and undergoes protease cleavage to become a mature enzyme (Pasternack et al. 1998). Pro-MTG is efficiently secreted by *Corynebacterium glutamicum* (*Corynebacterium* Expression System CORYNEX®; Ajinomoto Co., Inc., Tokyo, Japan), and subsequently activated by proteases (Date et al. 2003; Kikuchi et al. 2003). *C. glutamicum*, is non-pathogenic, does not produce toxins, and has been used for decades in the industrial production of amino acids such as glutamic acid and lysine. CORYNEX® is a suitable host for the secretory expression and industrial production of MTG.

MTG is used extensively in the food industry and has also attracted attention in the cosmetics, textiles and leather processing industries (Fontana et al. 2008; Zhu and Tramper. 2008). In addition, MTG has been used in the biomedical field, particularly in tissue engineering and antibody–drug conjugates (ADCs) (Chan and Lim. 2019; Deweid et al. 2019; Doti et al. 2020), and numerous other applications; however, success in the wider applications of MTG requires improvements in enzyme function.

We performed structure-based rational mutagenesis, in addition to random mutagenesis of the entire MTG gene region. These approaches produced 32 rational modification mutants and 10 random mutants each with higher specific activity than wild-type MTG. Furthermore, a mutant with an amino acid substitution from Ser to Ala (S199A), and also containing an N-terminal tetrapeptide, was found to be 1.7-fold more active than wild-type MTG (Yokoyama et al. 2010).

Marx et al. (2008) developed a screening method involving an activation step of soluble proenzymes expressed in *E. coli* and, to improve the thermostability of MTG, generated thermostable mutants by random mutagenesis, saturation mutagenesis and DNA shuffling (Buettner et al. 2012). A triple mutant S23V/Y24N/K294L showed a 12-fold higher half-life at 60 °C (t1/2 = 24.3 min) than wild-type MTG. Böhme et al. (2020) also produced 31 MTG mutants. The most thermostable mutants (S2P, S23Y, S24 N, H289Y, K294L) had a 19-fold longer half-life at 60 °C (t1/2 = 38 min) than wild-type MTG.

Wang et al. (2021) reported a thermostable mutant, FRAPD-TGm2 (FRAPD-TGm1-E28T-A265P-A287P), created by modifying the mutant FRAP-TGm1 (S2P, S23V, Y24N, S199A, K294L). The half-life, melting temperature (Tm) and specific activity of FRAPD-TGm2 were 66.9 min (t1/2(60 °C)), 67.8 °C and 71.8 U/mg, respectively, a twofold, 2.6 °C and 43.8% increase compared to FRAPD-TGm1. Further modification led to the discovery of FRAP-TGm2A (FRAPD-TGm2-S116A-S179L) with a half-life at 60 °C of 132.38 min (t1/2(60 °C)) and specific activity of 79.15 U/mg: 84% and 21% higher than FRAPD-TGm2, respectively (Yang et al. 2023).

Although mutants with improved thermostability have been obtained, further thermostability is required for use in industrial processes, such as in the heat deactivation process during food production. In our previous report (Suzuki et al. 2022), we produced a thermostable MTG mutant D3C/G283C based on structure-based disulfide (SS) bridge engineering. In this study, we obtained more thermostable MTG mutant than D3C/G283C MTG by random mutation screening using the thermostable mutant D3C/G283C as a template. Several amino acid substitutions were found to improve the thermostability of D3C/G283C MTG. The combination of multiple amino acid substitutions resulted in a mutant D3C/S101P/G157S/G250R/G283C with higher thermostability and specific activity compared to D3C/G283C MTG. We also determined the three-dimensional (3D) structure of D3C/G283C MTG using X-ray crystallography. The crystal structures of wild-type MTG (Kashiwagi et al. 2002) and D3C/G283C MTG were used to discuss the stabilization mechanism of each mutation; the determination of the 3D structure of D3C/G283C MTG will allow further thermal stabilization research to progress.

Materials and methods

Chemicals

HPLC grade solvents were purchased from Nacalai Tesque (Kyoto, Japan); TFA (analytical grade) was purchased from Wako Life Science (Osaka, Japan). Other chemicals were reagent grade.

Bacterial strains

E. coli JM109 purchased from Takara Bio (Kyoto, Japan) and *C. glutamicum* ATTC13689 were used in this study. *E. coli* JM109 was cultured in lysogeny broth (LB) containing a final concentration of 25 µg/mL kanamycin (Km) and used as an intermediate for various plasmid constructs and as a host for the random mutagenesis library.

Culture medium for *C. glutamicum*

C. glutamicum was grown in CM2G medium at 30°C. The pro-form production medium for *C. glutamicum* was used with MMTG medium at 30°C. The culture medium of *C. glutamicum* in this study contained 25µg/mL Km as the final concentration. To introduce an SS bridge into MTG, the reductant reagent dithiothreitol (DTT), final concentration 3 mM, was added to MMTG medium 7 h after starting cell culture (Yokoyama et al. 2021; Suzuki et al. 2022).

Plasmid

The thermostable mutant D3C/G283C expression vector pPSPTG-D3CG283C constructed from the Pro-MTG expression vector pPSPTG11 was used in this study (Suzuki et al. 2022).

DNA manipulations

All DNA manipulations followed standard procedures (Sambrook et al. 1989). PCR using Pyrobest DNA polymerase (Takara Bio, Kyoto, Japan) was performed in 50 µL reaction mixtures for 5 min at 94°C, for 25 cycles of 10 s at 98°C, 30 s at 55°C and 3 min at 72°C. Nucleotide sequences were determined using the BigDye Terminator Cycle Sequencing FS Ready Reaction Kit and DNA sequencer model 377 (Applied Biosystems, Waltham, United states of America).

Random mutagenesis of D3C/G283C MTG

Random mutagenesis was performed using the GeneMorph II Random Mutagenesis Kit (Stratagene California, La Jolla, United States of America), according to the manufacturers' instructions. Template DNA (5–20 ng pPSPTG-D3CG283C) were used in the error-prone PCR reaction. Mutation rates were controlled to be two or three base pairs in the D3C/G283C MTG coding region. The PCR primers were derived from sequences at the beginning and end of the D3C/G283C MTG gene (forward primer: 5'-tccatagcaatccaaagg-3', reverse primer: 5'-gggcgaccgagaagtttttttacaaaaggca-3'). After *Dpn*I treatment, the PCR product was purified, digested with both *EcoO*65I and *Bam*HI and purified again. The plasmid pPSPTG-D3CG283C was also digested with both *EcoO*65I and *Bam*HI. After restriction enzyme treatment, two DNA fragments were detected by agarose gel electrophoresis. The larger DNA fragment (about 7 Kb), derived from pPSPTG-D3CG283C, was purified, reacted with SAP (Shrimp alkaline phosphatase, Takara Bio, Kyoto, Japan), and purified again. The digested PCR product and the larger DNA fragment were ligated and transformed into *E. coli* JM109. Transformed cells were plated on LB plates containing 25 µg/mL Km, and the colonies formed were used for library screening.

Screening for thermostable candidates of D3C/G283C MTG mutants

Plasmids containing the screening library were transformed into *C. glutamicum* using electroporation, as described previously (Yokoyama et al. 2010). The transformed cells were plated onto CM2G plates containing 25 µg/mL Km and screened as follows: (i) A deepwell microtiter plate was filled with 1.0 mL CM2G medium per well. Each well was incubated with a single colony of transformed *C. glutamicum*. The deepwell microtiter plate was sealed with gas permeable adhesive seal and precultured in a shaking incubator at 1500 rpm, 30°C for 24 h. (ii) A deepwell microtiter plate was filled with 1.0 mL MMTG medium containing 25 µg/mL Km and 5.0 g/L $CaCO_3$ per well. Each well was incubated with 50 µL preculture medium. The plate was sealed as described above and cultured in a shaking incubator at 1500 rpm, 30°C. After 7 h, DTT at a final concentration of 3 mM was added to MMTG medium and cultured for 43 h. (iii) A deepwell microtiter plate containing cultured medium of the transformed cells was centrifuged at 3000 rpm, 4°C for 10 min. (iv) Supernatant (200 µL) containing the proform of D3C/G283C MTG mutants was diluted 5 times with 50 mM MOPS, pH 7.0 in a deepwell microtiter plate then activated by a protease, as described previously (Yokoyama et al. 2010). After activation, 100 µL of the supernatant was incubated with 1.0 mM phenylmethylsulfonyl fluoride (PMSF) at 25°C for 1 h in a deepwell plate. After PMSF treatment, the supernatant was incubated at 65°C for 10 min using the TaKaRa PCR Thermal Cycler Dice® Gradient (Takara Bio, Kyoto, Japan), then cooled down to 4°C. The MTG activity of the heat-shocked supernatant was assayed using a SpectraMax 340PC microplate reader (Molecular Devices, Sunnyvale, CA) and colorimetric hydroxamate procedure using N-carbobenzoxy-L-glutaminylglycine (Z-QG), as described previously (Yokoyama et al. 2010). The thermostable candidates of D3C/G283C MTG mutants with high residual activity were selected by comparing the ratio between non-incubated supernatant and heat-shocked supernatant at 65°C for 10 min.

Construction of Multiple Mutants of D3C/G283C MTG

Site-directed mutagenesis of the D3C/G283C MTG gene was performed using the QuickChange® II Site-Directed Mutagenesis Kit (Stratagene California, La Jolla, United States of America). The template DNA was pPSPTG-D3CG283C. Mutagenesis primers were designed according to the instructions of the mutagenesis kit, referring to the codon of *C. glutamicum.* After digestion with restriction enzyme *Dpn*I, the resulting plasmid containing the mutant gene was transformed into *E. coli* JM109. Transduction of the mutation was confirmed by DNA sequencing. The mutant plasmid was transformed into *C. glutamicum* and a mutant strain was prepared.

Evaluation of thermostable candidates of D3C/G283C MTG mutant

The thermostable candidate strains obtained above were inoculated into 3 mL CM2G medium containing 25 µg/

mL Km, and pre-cultured at 30°C. Next, 200 µL of the preculture solution was inoculated into 4 mL MMTG medium containing 25 µg/mL Km and 5.0 g/L $CaCO_3$ at 30°C. After 7 h, DTT, at a final concentration of 3 mM, was added to MMTG medium, then cultured for 43 h. Protease was added to the supernatant after centrifugation at 1/100 of MTG and reacted at 30 °C for 16 h. The buffer of the solution containing activated MTG was replaced with 20 mM sodium phosphate (pH 6.0) by PD-10 Desalting Column (GE Healthcare Bio-Sciences, Piscataway, United States of America). Thermostable candidates with high residual activity were selected by using the ratio of non-incubated supernatant to heat shock supernatant at 67 °C for 10 min.

Purification of D3C/G283C MTG mutants

Multiple mutants of D3C/G283C MTG were purified using a cation-exchange column RESOURCE S 6 ml (GE Healthcare UK Ltd., Hatfield, Great Britain) equilibrated with 20 mM sodium acetate (pH 5.5) (Suzuki et al. 2022). Collected fractions were applied to a PD-10 equilibrated with 20 mM 2-(N-morpholino) ethanesulfonic acid (MES) (pH 6.0), and proteins were eluted using the same buffer. Purified mutant fractions were frozen at -80 °C before use.

Determination of protein concentration

Analytical reverse-phase HPLC was performed using a Proteonavi C4 column (4.6 mm id × 15 cm, Shiseido), as described previously (Suzuki et al. 2022).

Determination of MTG activity

The specific MTG activity was measured with a colorimetric hydroxamate procedure using N-carbobenzoxy-L-glutaminylglycine (Z-QG), as described previously (Suzuki et al. 2022). Test sample (100 µL) was incubated with 1 mL of solution A for 10 min at 37, 45, 50, 55, 60, 65 and 68°C, respectively. The reaction was stopped by the addition of 1 mL solution B and the absorbance was measured at 525 nm. One unit was defined as the formation of 1 mol of hydroxamic acid per min using L-glutamic acid γ-monohydroxamate as the standard.

Thermal stability determination

Thermal stability was described as T_{50} being the temperature of incubation at which 50% of the initial activity remains (Mansfeld et al. 1997).

Kinetic parameter measurements

Measurement of the kinetic parameter for MTG was performed using a GDH-coupled enzyme assay, as described previously (Day and Keillor 1999; Oteng-Pabi and Keillor 2013). The optimized assay was performed as described previously (Suzuki et al. 2022).

Sample preparation of D3C/G283C MTG for crystallization

The protein solution for the crystallization of D3C/G283C MTG was prepared as described previously (Suzuki et al. 2022). The experimental details, including the culture medium for *C. glutamicum* ATTC13689, almost all of the protein purification protocol, and the determination of protein concentration were the same as those for the D3C/G283C MTG mutants mentioned above. The final purified protein solution, in which the buffer was exchanged to 20 mM phosphate (pH 6.0) and the protein concentration was adjusted to 1 mg/mL, was frozen at -80°C before use.

Crystallization of D3C/G283C MTG

Just before crystallization, the purified sample of D3C/G283C MTG was rapidly thawed in an ice bath, exchanged to a buffer containing 10 mM acetate (pH 5.0), and concentrated to ~ 15 mg/mL using an Amicon Ultra Centrifugal Filter with a molecular weight cut-off of 10 kDa (Merck, Darmstadt, Germany). Crystallization of D3C/G283C MTG was performed using the hanging-drop mode of the vapor-diffusion method at 293 K. The crystallization solution in the reservoir had a volume of 500 µL and was composed of 25% w/v polyethylene glycol (PEG) 1000, 100 mM MES-NaOH buffer (pH5.0), and 25 mM $CaCl_2$. One µL of D3C/G283C MTG solution (~ 15 mg/mL) and 1 µL of the crystallization solution were mixed and then equilibrated against the reservoir.

Data collection and structure determination of D3C/G283C MTG crystal

X-ray diffraction datasets of the obtained crystals of D3C/G283C MTG were collected using ADSC Q210 CCD detector (Area Detector Systems Corporation, Poway CA, United states of America) on the beamline NW12A of Photon Factory—Advanced Ring for Pulse X-rays (PF-AR) at the High Energy Accelerator Research Organization (Tsukuba, Japan). During the collection of the X-ray diffraction data, the MTG crystal was flash-cooled at 100 K after equilibration against a cryo-solvent containing 35% w/v PEG 1000, 120 mM MES-NaOH buffer (pH5.0), and 35 mM $CaCl_2$. The X-ray wavelength was set to 1.000 Å, and the diffraction path

was filled with He gas to avoid air scattering. The diffraction datasets were processed using the program XDS (Kabsch 1993). Initial structural model of D3C/G283C MTG was determined by the molecular replacement (MR) method using the program AMoRe (Navaza 1994) in the CCP4 package (Winn et al. 2011). Subsequently, manual model rebuilding using the program Coot (Emsley and Cowtan 2004) and crystallographic refinement using the program Refmac5 (Murshudov et al. 1997) were iteratively performed. The final structures were validated by the Protein Data Bank (PDB) validation server (https://validate-rcsb.wwpdb.org/). The figure preparation presenting 3D structures and the model construction of Ab2c2 MTG were performed using the programs Discovery Studio Visualizer (https://www.3ds.com) and Coot.

Results

Screening of a random mutant library of D3C/G283C MTG and identification of amino acid substitutions effective for improving thermostability

Mutations were introduced into the region encoding the active form of MTG by the error-prone PCR. The secretion and activity of MTG (by analytical reverse-phase HPLC and a colorimetric hydroxamate procedure, respectively) was then determined in approximately 10,000 mutant strains. Proteases added for activation were inhibited using PMSF, and samples were heat shocked at 65 °C before activity measurement. Those showing residual activity equal to or greater than that of D3C/283C MTG were selected, and those with reduced secretion of MTG (secretion of less than 0.3 mg/ml) and those with reduced specific activity at 37 °C (ratio of specific activity to wild type less than 0.6) were excluded. The results are summarized in Table 1 in the order of highest to lowest residual activity. Amino acid substitutions S101P, V112I/G250R, A83T, N92S/G250R, T53S/G157S, G157A, N92D/G250R, and G250A improved the thermostability of D3C/G283C MTG without reducing secretion or specific activity (Table 1). We then investigated whether multiple combinations of these amino acid substitutions could further improve the thermostability without reducing secretion or specific activity.

Introduction of multiple amino acid substitutions into D3C/G283C MTG and evaluation of thermostability

We introduced multiple amino acid substitutions into D3C/G283C MTG, always using S101P, which had the highest thermostability of the single mutations. Further mutants were created by adding G250(A, R), G157(A, S), T53S, A83T, N92S, and V112I in this order, as shown in Figure S1. Mutants containing G250R, G250A, G157S and G157A improved heat resistance (Table 1): suggesting that amino acid substitutions to G250 and G157, in addition to S101P, are also useful for improving heat resistance. In total, we investigated 23 mutants with high thermostability, and measured the residual activity and secreted amount (Table 2). Heat resistance increased accumulatively with combinations of S101P, G250A, R and G157A, S. However, there was no further increase in thermostability in samples with further mutation points, and many showed a decrease in secretion. Based on these results, we decided to further investigate four mutants: Ab1c1 (D3C/G283C, S101P, G250A, G157A), Ab1c2 (D3C/G283C, S101P, G250A, G157S), Ab2c1 (D3C/G283C, S101P, G250R, G157A), and Ab2c2 (D3C/G283C, S101P, G250R, G157S) (Table 2).

Table 1 Residual activity after heat shock, TG secretion and relative activity of wild-type, D3C/G283C and mutants and amino acid substitutions due to mutation

Amino Acid Substitution	Residual Activity at 65 °C	TG secretion	Relative Activity at 37 °C
	Ratio	mg/mL	Ratio
Wild-type MTG	0.038	0.59	1.00
D3C/G283C	0.064	0.37	1.06
S101P	0.541	0.32	0.96
V112I/G250R	0.495	0.35	0.98
A83T	0.490	0.31	0.60
N92S/G250R	0.421	0.36	1.17
T53S/G157S	0.411	0.38	1.01
G157A	0.409	0.35	0.97
G250A	0.391	0.35	1.27
G250E	0.226	0.30	0.72
T53S	0.201	0.33	1.52
N92D/G250R	0.188	0.36	1.33
R79S	0.144	0.36	0.68
A267V	0.130	0.30	1.01
N297K	0.104	0.30	0.92

The ratio of residual activity was calculated between non-incubated supernatant and heat-shocked supernatant at 65°C for 10 min. Secretion of protein was determined by analytical reverse-phase HPLC. The ratio of relative activity was calculated between mutants and wild-type

Preparation of purified enzymes from four D3C/G283C MTG mutants and detailed evaluation of thermostability

The specific activity and residual activity after heat shock were determined in four mutants, Ab1c1, Ab1c2, Ab2c1, and Ab2c2, and D3C/G283C after purification by cation exchange resin. Ab2c2 showed the highest specific activity

Table 2 Residual activity after heat shock of mutants of amino acid substitution to D3C/G283C MTG, and TG secretion

Mutation	Enzyme	Residual Activity at 67 °C	TG secretion
		Ratio	mg/mL
Parent	D3C/G283C	0.02	0.31
Single	A	0.04	0.33
Double	Ab1	0.19	0.23
	Ab2	0.41	0.20
Triple	Ab1c1	0.45	0.45
	Ab1c2	0.47	0.44
	Ab2c1	0.43	0.46
	Ab2c2	0.53	0.45
Quadruple	Ab1c1D	0.40	0.04
	Ab1c2D	0.31	0.04
	Ab2c1D	0.49	0.24
	Ab2c2D	0.38	0.05
Fivefold	Ab1c1DE	N.D	0.05
	Ab1c2DE	N.D	0.03
	Ab2c1DE	0.02	0.20
	Ab2c2DE	0.03	0.29
Sixfold	Ab1c1DEF	N.D	0.30
	Ab1c2DEF	N.D	0.26
	Ab2c1DEF	N.D	0.20
	Ab2c2DEF	N.D	0.26
Sevenfold	Ab1c1DEFG	N.D	0.23
	Ab1c2DEFG	0.03	0.18
	Ab2c1DEFG	0.03	0.19
	Ab2c2DEFG	0.25	0.14

The ratio of residual activity was calculated between non-incubated sample and heat-shocked sample at 67°C for 10 min. Secreted protein was determined by analytical reverse-phase HPLC

Table 3 The specific activity of wild-type MTG, D3C/G283C and the multiple D3C/G283C MTG mutants

Enzyme	Specific Activity (37°C)
	U/mg
Wild-type MTG	26.7
D3C/G283C	34.6
Ab1c1	39.5
Ab1c2	38.6
Ab2c1	26.7
Ab2c2	41.1

The specific activity was measured by hydroxamate assay, as described in the Materials and Methods

at 37 °C of 41.1 U/mg compared to 34.6 U/mg for D3C/G283 MTG (Table 3). Residual activity was measured after thermal shock at 63.6, 64.2, 66.8, 68.2, 69.7, and 71.1 °C. The four mutants clearly showed higher residual activity than D3C/G283C MTG, ranging from 66.8°C to 68.2°C (Fig. 1). Ab1c2, Ab2c1, and Ab2c2, maintained enzyme activity at a ratio of 0.4 to 0.5 at 68.2°C compared to 0.03 for D3C/G283C MTG. All mutants lost enzyme activity at 71.1°C. We then further characterized Ab2c2 (D3C/G283C, S101P, G250R, G157S) since it was the most thermostable mutant and had the highest specific activity.

Evaluation of thermostability, temperature dependence of activity and kinetic parameters of Ab2c2 MTG

The thermal stability of Ab2c2 MTG, D3C/G283C MTG, and wild-type MTG, was determined after heat-shock at temperatures between 25°C to 70°C, to determine residual activity at 37 °C and *T50* values. Ab2c2 MTG had a ΔT_{50} increase of + 1°C compared to D3C/G283C MTG (Table 4).

The temperature dependence of activity was evaluated by measuring specific activity at any temperature from 37 °C to 68 °C (Fig. 2). The specific activity of Ab2c2 MTG showed a maximum value of 115 U/mg at 65°C. Wild-type MTG showed 45 U/mg at 55°C and D3C/G283C MTG showed 75 U/mg at 60°C, indicating that Ab2c2 MTG has extremely

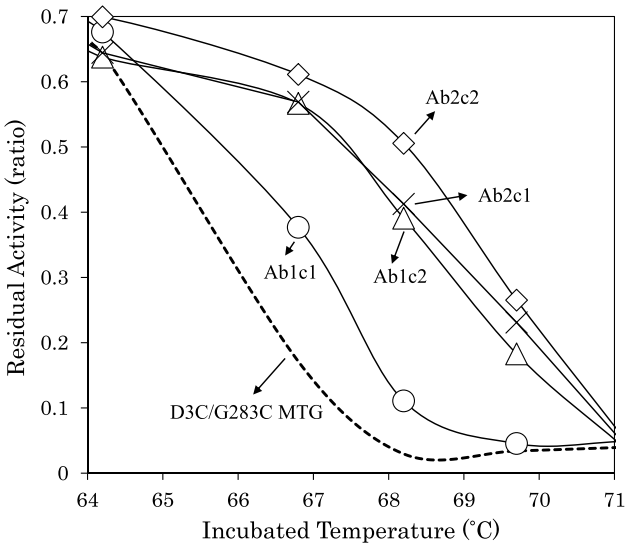

Fig. 1 Residual activity of D3C/G283C and multiple mutants after heat shock; D3C/G283C MTG (dotted line), Ab1c1 (open circle), Ab1c2 (open triangle), Ab2c1 (cross) and Ab2c2 (open square). Enzymes were treated at 63.6, 64.2, 66.8, 68.2, 69.7, and 71.1 °C for 10 min, prior to activity measurement. The ratio of residual activity was calculated between non-incubated sample and heat-shocked sample

Table 4 Measurement of the T_{50} value and kinetic constant at 37 °C of wild-type, D3C/G283C and Ab2c2 MTG

Enzyme	T_{50} °C	ΔT_{50}	V_{max} μmol/min/mg	K_m mM	k_{cat} s^{-1}	k_{cat}/K_m M^{-1} s^{-1}
Wild-type MTG	57.2	0	0.53 ± 0.07	1.07 ± 0.40	0.34 ± 0.045	332 ± 80
D3C/G283C	66.1	+ 8.9	0.49 ± 0.02	0.82 ± 0.14	0.31 ± 0.011	387 ± 55
Ab2c2	67.3	+ 10.1	0.75 ± 0.07	0.95 ± 0.44	0.47 ± 0.043	590 ± 143

T_{50} is defined as the temperature of incubation at which 50% of the initial activity of the enzyme solution remained. ΔT_{50} values represent the difference between wild-type MTG and mutant enzymes

Assay of kinetic constants were carried out as described in Materials and Methods. Data were expressed as mean ± SD (n = 3)

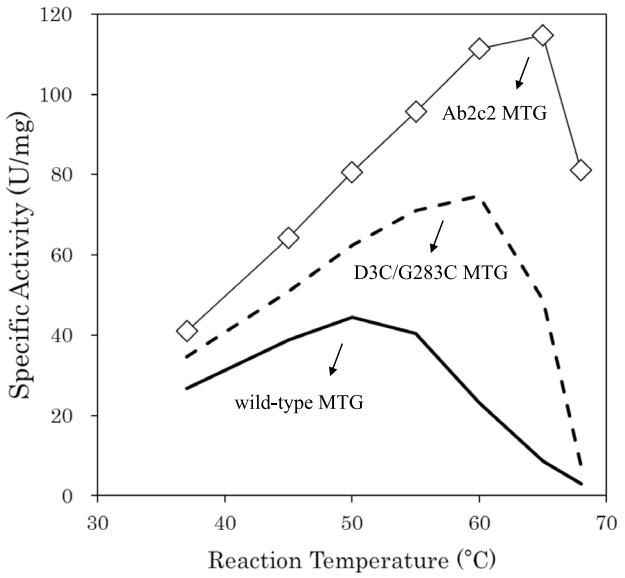

Fig. 2 Temperature dependence of specific activity of wild-type MTG (solid line), D3C/G283C MTG (dotted line), and Ab2c2 MTG (open square). Specific activities were measured using the hydroxamate assay in the temperature range from 25 °C to 68 °C for 10 min

high specific activity and thermostability compared to D3C/G283C and wild-type MTG.

Enzyme kinetics of the thermostable mutants Ab2c2 MTG, D3C/G283C MTG and wild type MTG were determined using a GDH binding enzyme assay. The K_m values were not significantly different between the three enzymes; however, Ab2c2 MTG had approximately 1.4-fold higher k_{cat} and V_{max} values compared to wild-type MTG. The k_{cat}/K_m value of Ab2c2 was increased to 590 ± 143 M^{-1} s^{-1}, which was approximately 1.8 times higher than those of D3C/G283C and wild-type MTG (Table 4).

These results suggest that disulfide bridge formation (D3C/G283C) and triple mutations (S101P, G250R, G157S) contribute to the improved heat resistance. On the other hand, Marx et al. (2008) obtained six mutants (S2P, S23Y-Y24N, G257S, K269S, H289Y, and K294L) with improved thermostability by random mutation of wild-type MTG, but the results were different from those obtained by introducing random mutations into disulfide mutants. Structural analysis of the disulfide transgenic mutants was considered necessary to elucidate this difference and for further modification in the future.

Crystallization, data collection and structure determination of D3C/G283C MTG crystal

D3C/G283C MTG was crystallized under almost the same conditions as wild-type MTG (Kashiwagi et al. 2002). A few days after the start of crystallization, plate-like crystals of D3C/G283C MTG emerged and grew to a size (0.4 × 0.2 × 0.1 mm) sufficient for X-ray diffraction. Data collection of D3C/G283C MTG crystals was performed on the beamline PF-AR NW12A (Table S1). The resulting crystal form of D3C/G283C MTG was almost identical to that of the wild-type MTG.

The initial structure of D3C/G283C MTG was constructed using the MR method using the structure of wild-type MTG (Kashiwagi et al. 2002) (PDB ID: 1IU4_A) as a search model. In the asymmetric unit of the crystal, the MR method successfully found four independent MTG molecules which corresponded well to the molecules A, B, C, and D of the wild-type MTG. Next, manual model building and crystallographic refinement were iteratively performed. Because the electron density of amino acid residues 3 and 283 in each protein molecule apparently demonstrated that both of two residues were mutated to Cys and their side-chains were disulfide bonded to each other, the protein structure was corrected accordingly (Fig. 3). Finally, the structure of D3C/G283C MTG was determined at 2.0 Å resolution (Table S1). The coordinate data and the structure-factor dataset of D3C/G283C MTG have been deposited in the PDB with PDB ID of 9IHS.

3D structure of D3C/G283C MTG

The overall 3D structure of D3C/G283C MTG was almost identical to the wild-type MTG (Fig. 4a). Two protrusions P-1 and P-2 constructed the active site cleft where the catalytic residue

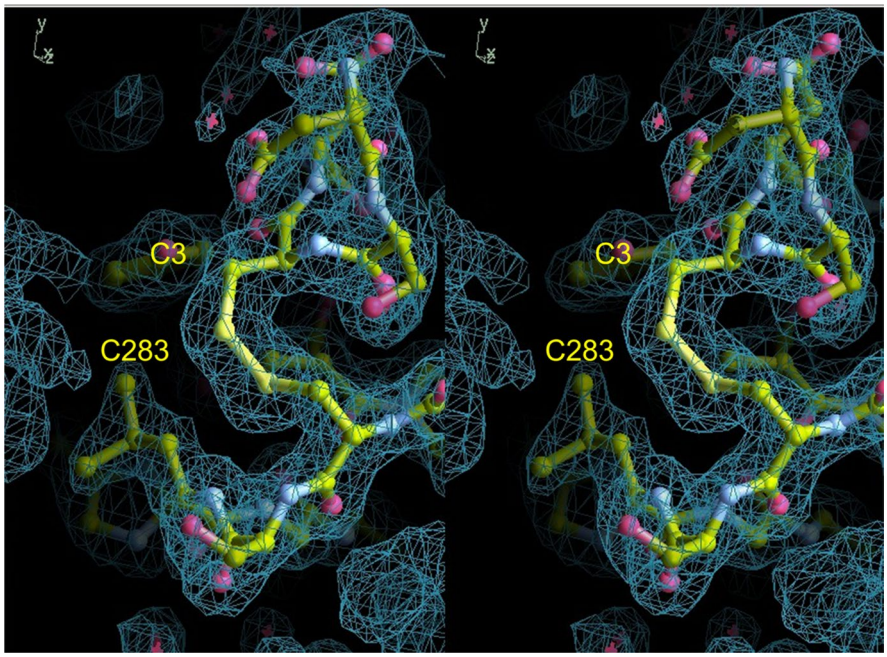

Fig. 3 Stereo view of the disulfide bond in D3C/G283C MTG. Protein structure around Cys3 and Cys283 in the molecule C is drawn using a ball-and-stick model. The (2Fo-Fc) difference Fourier electron-density map contoured at 1σ is superimposed on the protein structure

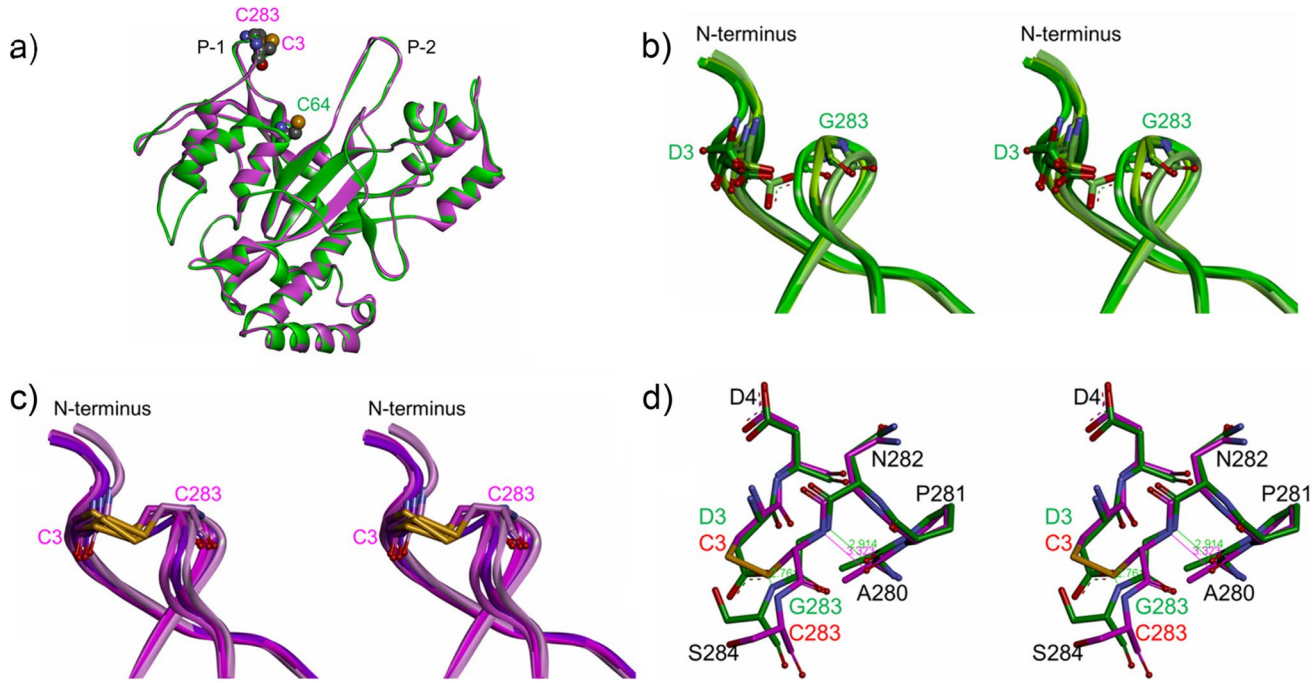

Fig. 4 Structural comparisons between wild-type MTG and D3C/G283C MTG. The structures of wild-type MTG and D3C/G283C MTG are shown in green and purple, respectively. **a** Superimposed ribbon models (front views) of the overall structures of the MTG molecules B in both crystal structures. The mutated residues C3 and C283 in D3C/G283C MTG and the catalytic residue C64 in wild-type MTG are shown with sphere models. Labels P-1 and P-2 indicate two protrusions which construct the active site cleft. **b** Superimposed ribbon models of protrusions P-1 of the MTG molecules A, B, C, and D in the wild-type MTG crystal structure (stereo view). Residues D3 and G283 are shown with stick models. In the order of A, B, C, and D, the green color scheme of the molecule changes from dark to light. **c** Superimposed ribbon models of protrusions P-1 of the MTG molecules A, B, C, and D in the D3C/G283C MTG crystal structure (stereo view). Residues C3 and C283 are shown with stick models. In the order of A, B, C, and D, the purple color scheme of the molecule changes from dark to light. **d** Superimposed stick models of the structures around the mutation sites of the MTG molecules A in both crystal structures (stereo view). Hydrogen bonds observed only in the wild-type MTG crystal structure are represented with green lines accompanied by the atomic distances (Å unit). Corresponding atomic distance in the D3C/G283C MTG is represented with purple line and character

C64 exists at the base (Kashiwagi et al. 2002). Protrusion P-1 consists of two loop structures (D1-A10 and N276-M288), and the two mutation sites of D3C/G283C MTG ride on these two loops. The protrusion P-2 consists of a single long loop structure (D233- N255). The residue G250, which is one of the mutation sites in Ab2c2 MTG, resides within this loop.

In both crystal structures of wild-type and D3C/G283C MTGs, slightly larger conformational variation between the four independent MTG molecules (A, B, C, and D) was observed around the mutation sites of the D3C/G283C MTG (Fig. 4b and c). In most cases, structural comparisons of the MTG molecules in the same crystal structure demonstrated that the RMSD values of Cα displacement in this region (residues 2–4 and 282–284) were greater than those for the whole molecule (Table S2). The main cause of this phenomenon is suggested to be due to crystal packing. In the asymmetric unit of the MTG crystal, the four MTG molecules interacted with each other to form a tetramer (Fig. 5a). Interestingly, two protrusions P-1 and P-2 formed the intermolecular contact interfaces in the MTG tetramer, and the residues around the mutation sites in the MTG molecules A, B, C, and D existed closely to the neighboring MTG molecules C, D, A, and B, respectively (Fig. 5b and c). Residue S101, a mutation site of Ab2c2 MTG, E107, and Y217 in the neighboring MTG molecule were representative residues involved in packing interactions within the vicinity of mutation sites of D3C/G283C MTG. Among the four vicinities around the mutation sites of MTG molecules A, B, C, and D, MTG molecule A was the least affected by crystal packing (Table S2, Fig. 5b and c).

Therefore, the MTG molecules A of wild-type MTG and D3C/G283C MTG were selected for a detailed structural comparison around the mutation sites (Fig. 4d). The conformation of the residues around the mutation sites in D3C/G283C MTG was similar to that of wild-type MTG. The interatomic interaction within this region was similar between the structures of wild-type and D3C/G283C MTGs, except that two hydrogen bonds present in wild-type MTG were lost in D3C/G283C MTG. One was a hydrogen bond between D3 O_{δ} and S284 N, which was inevitably lost because of the D3C mutation. The other was a hydrogen bond between A280 O and G283 N, which might be lost because of the structural distortion caused by the disulfide bond. These two hydrogen bonds were also not observed in molecules B, C, and D in D3C/G283C MTG, suggesting that two lost hydrogen bonds were significant structural changes between the two MTG structures.

Discussion

In this study, the introduction of multiple amino acid substitutions, by random mutation, improved thermostability in D3C/G283C MTG, up to a point: the triple mutation S101P, G250R, G157S showed an accumulative improvement in thermostability, however, when further mutations (T53S, A83T, N92S, and V112I) were introduced, no further increase in thermostability was observed, and in many cases, the secretion level decreased. We selected for random mutations which introduced disulfide bonds and amino acid substitutions which contributed to improved heat resistance.

The Ab2c2 mutant (D3C/S101P/G157S/G250R/G283C) had extremely high thermostability and specific activity compared to D3C/G283C MTG and wild-type MTG. The previous thermostable mutant was structurally stable at 65 °C, but showed only about 16% of the specific activity of wild-type MTG (Böhme et al. 2020). In contrast, Ab2c2 MTG exhibited enzymatic activity (but not structural stability) at 67°C and specific activity at 37°C was 1.5 times higher than that of wild-type MTG. Furthermore, the optimal temperature for Ab2c2 MTG was 65°C, which was much higher than the 50° of wild-type MTG (Fig. 2). Further studies to increase the thermostability as well as enzymatic activity of MTG would be useful for industrial applications.

We were unable to obtain high quality crystals sufficient for structure determination of the Ab2c2 MTG mutant. The G250 residue, which is mutated to Arg in Ab2c2 MTG, exists on protrusion P-2 (Fig. 6a) (Kashiwagi et al. 2002). Interestingly, the P-2 protrusion formed the intermolecular contact interfaces in the MTG tetramer, and two G250 residues in the MTG molecules A and C (or B and D) exist in close proximity to each other (Fig. 6b and c). The positively charged bulky side chain of R250 may inhibit formation of the tetramer in the MTG crystal, which may explain the failure to obtain high-quality crystals of Ab2c2 MTG.

Microgravity environments have been utilized to obtain enhanced quality crystals because of the lack of gravity-induced convection (Mcpherson and DeLucas 2015). To analyze the structure of MTG with higher resolution, wild-type MTG and D3C/G283C MTG were crystallized utilizing superconducting magnet-based quasi-microgravity environments (Nakamura et al. 2012). However, no improvement in crystal quality was observed (unpublished data). MTG crystal growth is a complex process, requiring the formation of tetramers, this may have influenced the results.

The SS bridge in a protein molecule restricts the conformation of the unfolded state and reduces the entropy. Therefore, as long as the newly constructed SS bridge does not distort the protein structure of the folded state, it is expected that introduction of an SS bridge will stabilize the folded state. Since there was almost no structural difference between D3C/G283C MTG and wild-type MTG, it is likely that the main factor in the increased thermostability of D3C/G283C MTG is a decrease in entropy in the unfolded state. Two hydrogen bonds present in wild-type MTG were not present in the region of the mutation site of D3C/G283C MTG. The structural destabilization caused by

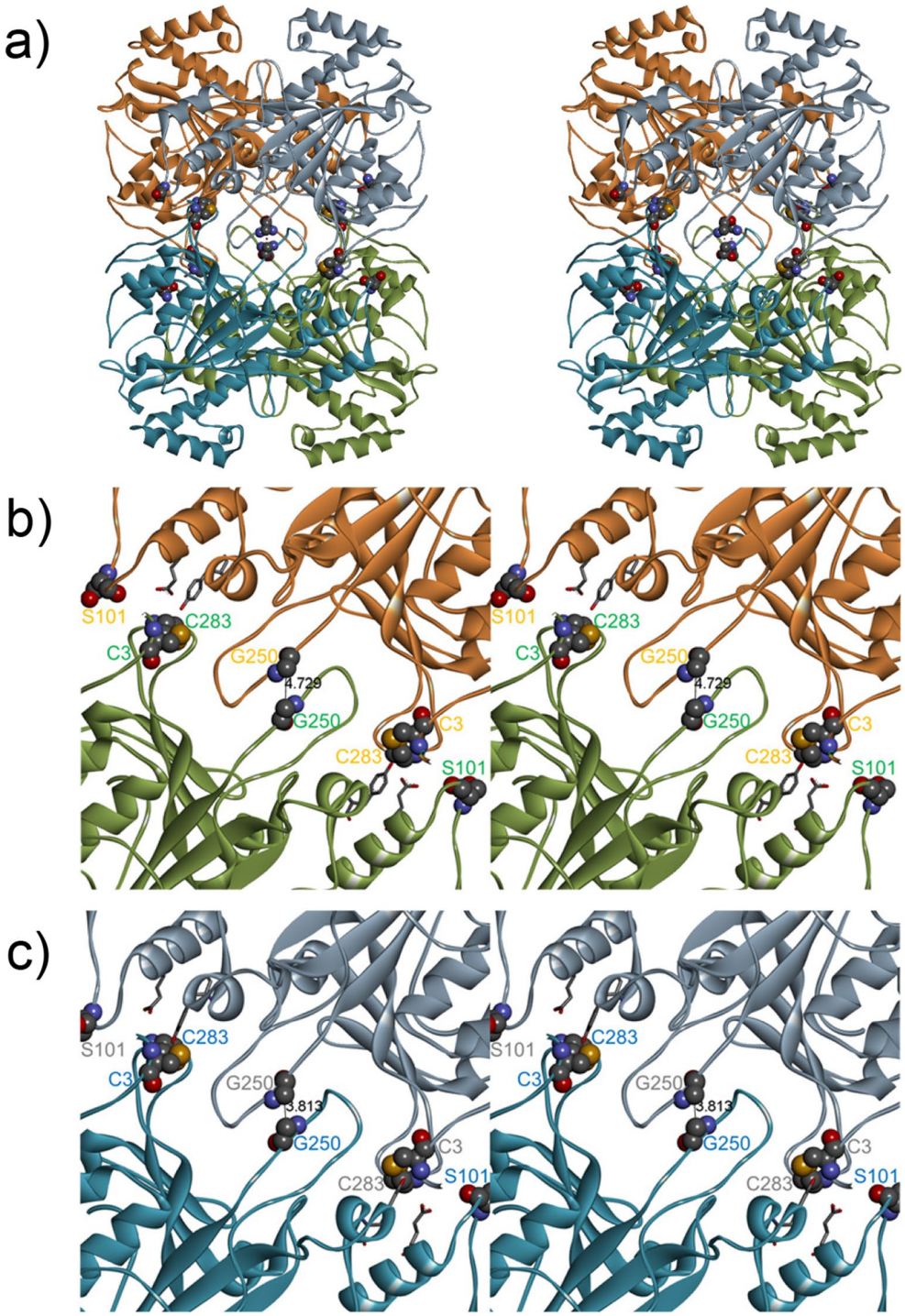

Fig. 5 Crystal packing interaction between the protrusions of the MTG molecules in the D3C/G283C MTG crystal structure. Four independent MTG molecules A, B, C, and D in the asymmetric unit are shown in green, blue, orange, and grey, respectively. Residues C3, S101, G250, and C283 are shown with sphere models. **a** Overall view of the asymmetric unit in the D3C/G283C MTG crystal structure (stereo view). **b** The interface between MTG molecules A and C (stereo view). **c** The interface between MTG molecules B and D (stereo view). In figures (**b**) and (**c**), the atomic distances (Å unit) between Cα atoms of residues G250 are represented with black line and characters. The residues E107 and Y217, which are representative residues that form crystal packing interactions with residues around the SS-bridge, are shown with stick models

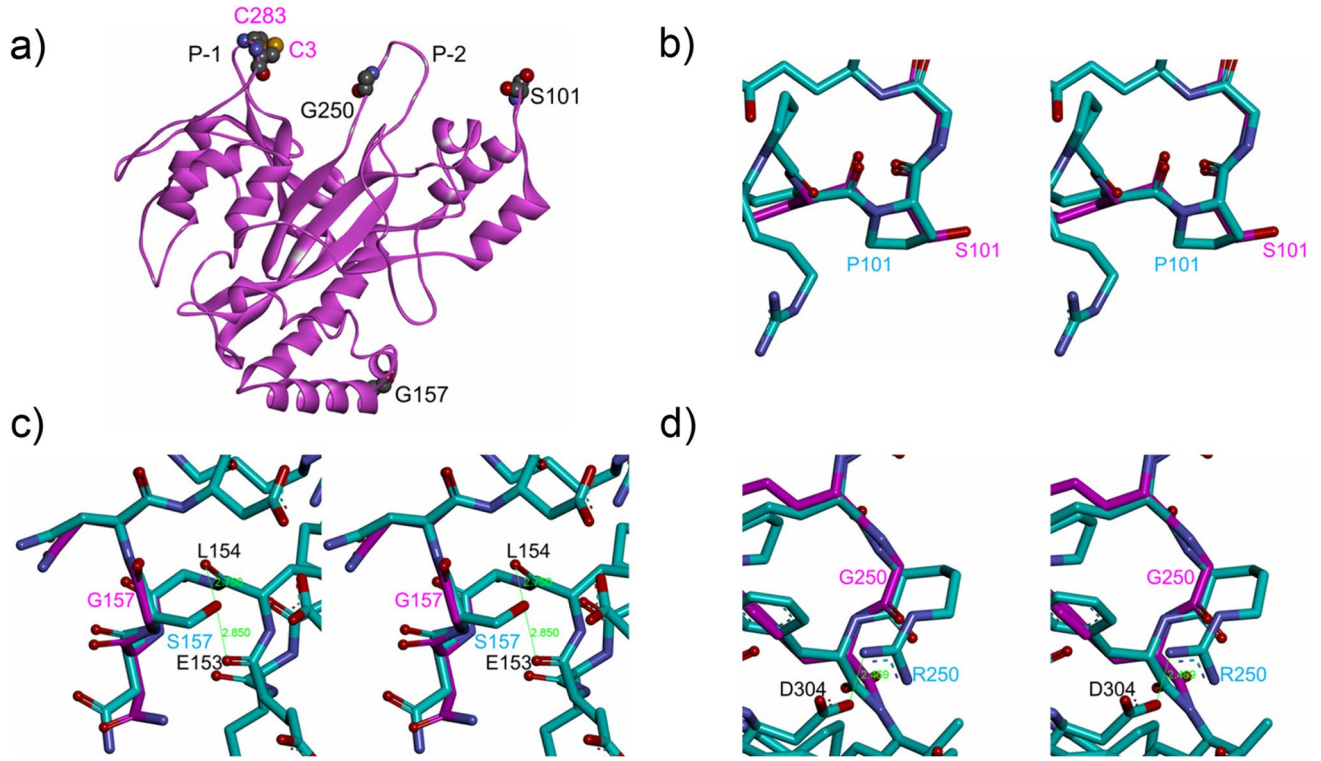

Fig. 6 Simulated structure of Ab2c2 MTG. **a** A ribbon model (purple) of the overall structure of D3C/G283C MTG molecules B. The mutated residues C3 and C283 and three additional mutation sites (S101, G157, and G250) in Ab2c2 MTG are shown with sphere models. Labels P-1 and P-2 indicate two protrusions which construct the active site cleft. **b**, **c**, and (**d**) Superimposed stick models (stereo view) of the simulated structure of Ab2c2 MTG (blue) and the crystal structure of D3C/G283C MTG (purple), around the mutated residues 101, 157, and 250. Putative hydrogen bonds and salt bridge observed in the simulated structure of Ab2c2 MTG are represented with green lines accompanied by the atomic distances (Å unit)

this loss might be sufficiently counteracted by the effect of entropy reduction in the unfolded state and direct structural stabilization by the formation of an SS bridge, a covalent bond between sulfur atoms of Cys residues.

It has been demonstrated that the greater the number of amino acid residues (N) between the two Cys which form the SS bridge, the greater the thermostability (Pace et al. 1988; Matsumura et al. 1989). The mutant T7C/E57C MTG (N = 49) has an SS bridge near the base of protrusion P-1 and shows higher thermostability than wild-type MTG ($\Delta T_{50} = +5$ °C) (Suzuki et al. 2022). The degree of improvement in the thermostability of T7C/E57C MTG is lower than that of D3C/G283C MTG (N = 279), which supports these findings.

Compared with wild-type MTG, D3C/G283C MTG not only showed improved thermostability, but also significantly improved specific activity at room temperature (Table 3). Around the mutation sites (residues 2–4 and 282–284) in both MTGs, the structural variation between the four MTG molecules in the asymmetric unit of the crystal was relatively large, possibly due to crystal packing. Interestingly, this tendency was more pronounced in wild-type MTG than in D3C/G283C MTG (Fig. 5b and c). The average RMSD values of Cα displacement between two MTG molecules (6 pairs) in the crystal structures of wild-type MTG and D3C/G283C MTG were 1.02 Å and 0.70 Å, respectively (Table S2). These results suggest that protrusion P-1 of D3C/G283C MTG is more rigid to external structural stress than P-1 in wild-type MTG. Since the N-terminus, which is a part of protrusion P-1, is known to affect the activity of MTG (Shimba et al. 2002), the increased rigidity of protrusion P-1 in D3C/G283C MTG may be related to the enhanced catalytic efficiency of this mutant.

In Ab2c2 MTG, three additional mutations, S101P, G157S, and G250R were introduced into D3C/G283C MTG. All of these mutations contributed to the enhanced thermostability. The three mutated residues are dispersed over the entire surface of the MTG molecule (Fig. 6a). Residue S101 was located on a loop present opposite the active site cleft with protrusion P-2 in between. Residue G157 was located on a small loop at the bottom of the MTG molecule. Residue G250 was located on protrusion P-2, as mentioned above. In the crystal structure of D3C/G283C MTG, the main chain dihedral angles (φ, ψ) of residues S101, G157, and G250

of every MTG molecule existed within the region allowed by Pro, Ser, and Arg, respectively, implying that these three mutations are unlikely to distort the main chain structure of the MTG molecule.

In the crystal structure of D3C/G283C MTG, residue S101 in every MTG molecule did not form intramolecular hydrogen bonds with its side chain (Fig. 6b). Therefore, mutagenesis from Ser to Pro at residue 101 is unlikely to destabilize the structure of the MTG molecule. Some Pro residues are considered to enhance the thermostability of proteins by decreasing entropy in the unfolded state (Ishikawa et al. 1993). The S101P mutation may enhance thermostability through this mechanism.

In the model structure of G157S, the side chain of S157 seemed to form a hydrogen bond with E153 O or L154 O (Fig. 6c), implying that mutagenesis from Gly to Ser at residue 157 stabilized the protein structure by the newly introduced hydrogen bond.

In the model structure of G250R, if it is allowed that the side chain of R250 adopts a minor rotamer, it could form a salt bridge with the side chain of D304 (Fig. 6d). Mutagenesis from Gly to Arg at residue 250 may stabilize the protein structure by the newly introduced salt bridge.

Although all of these mutations contributed to the enhanced thermostability, the degree of the effect seemed to be in the order of G250R > G157S > S101P. This tendency does not contradict the speculated mechanism for acquired thermostability of each mutant, as described above.

A previous study reported six mutants (S2P, S23Y-Y24N, G257S, K269S, H289Y, and K294L) with improved thermostability, obtained by introducing random mutations into wild-type MTG (Marx et al. 2008). Although some of these seven mutations have been demonstrated to play key roles for more improved thermostable mutants of wild-type MTG (Buettner et al. 2012; Böhme et al. 2020; Wang et al. 2021; and Yang et al. 2023), none of them were detected in the results of our current study.

S2P is suggested to contribute to the acquisition of thermostability by stabilizing the structure of protrusion P-1 including the N-terminus, as well as the introduction of disulfide bonds in D3C/G283C MTG. We can assume that this effect of S2P was not apparent in the random mutation to D3C/G283C.

Whereas residues S23, Y24, G257, K269, H289, and K294 are clustered at the right side of rear vestibule of the active site cleft (Figure S2). In the mutagenesis studies of wild-type MTG (Marx et al. 2008; Buettner et al. 2012; Böhme et al. 2020; Wang et al. 2021; and Yang et al. 2023), wild-type MTG which contained a FRAP sequence at its N-terminus and a His6-tag at its C-terminus, was used as a template. However, D3C/G283C MTG used in our current study, contains neither a FRAP sequence at its N-terminus nor a His6-tag at its C-terminus. Interestingly, the cluster of residues S23, Y24, G257, K269, H289, and K294 are located relatively close to the C-terminus of MTG (Figure S2).

Supplementary Information The online version contains supplementary material available at https://doi.org/10.1007/s00253-024-13304-1.

Acknowledgements Structure determination of D3C/G283C MTG

The work was performed under the approval of the Photon Factory Program Advisory Committee. We thank the Beamline staff members at KEK-PF for their assistance with data collection. This work was partly supported by the "Development of Systems and Technology for Advanced Measurement and Analysis (Program-S)" Fund of the Japan Science and Technology Agency. We thank Ms. Kobayashi R (WDB co. ltd.) for her technical assistance.

Authors' contributions KY conceived and designed research. MS, MD, KT and TK conducted the experiments. AN and MT assisted the use of a quasi-microgravity device. TK analyzed the structural data. ES contributed supervision and funding acquisition of structural analysis. MS, TK and KY wrote the manuscript. All authors read and approved the manuscript.

Funding This study was supported by Ajinomoto Co., Inc.

Data availability Not applicable.

Code availability Not applicable.

Declarations

Ethics approval This article does not contain any studies with human participants or animals performed by any of the authors.

Consent to participate Not applicable.

Consent for publication Not applicable.

Conflicts of interest/Competing interests This study was supported by Ajinomoto Co, Inc.

References

Ando H, Adachi M, Umeda K, Matsuura A, Nonaka M, Uchio R, Tanaka H, Motoki M (1989) Purification and characterization of a novel transglutaminase derived from microorganisms. Agric Biol Chem 53:2613–2617

Böhme B, Moritz B, Wendler J, Hertel TC, Ihling C, Brandt W, Pietzsch M (2020) Enzymatic activity and thermoresistance of improved microbial transglutaminase variants. Amino Acids 52:313–326

Buettner K, Hertel TC, Pietzsch M (2012) Increased thermostability of microbial transglutaminase by combination of several hot spots evolved by random and saturation mutagenesis. Amino Acids 42:987–996

Chan SK, Lim TS (2019) Bioengineering of microbial transglutaminase for biomedical applications. Appl Microbiol Biotechnol 103:2973–2984

Date M, Yokoyama K, Umezawa Y, Matsui H, Kikuchi Y (2003) Production of native-type *Streptoverticillium mobaraense* transglutaminase in *Corynebacterium glutamicum*. Appl Environ Microbiol 69:3011–3014

Day N, Keillor JW (1999) A continuous spectrophotometric linked enzyme assay for transglutaminase activity. Anal Biochem 274:141–144

Deweid L, Avrutina O, Kolmar H (2019) Microbial transglutaminase for biotechnological and biomedical engineering. Biol Chem 400:257–274

Doti N, Caporale A, Monti A, Sandomenico A, Selis F, Ruvo M (2020) A recent update on the use of microbial transglutaminase for the generation of biotherapeutics. World J Microbiol Biotechnol 36:53

Emsley P, Cowtan K (2004) Coot: model-building tools for molecular graphics. Acta Crystallogr D Biol Crystallogr 60:2126–2132

Folk JE (1980) Transglutaminases. Annu Rev Biochem 49:517–531

Fontana A, Spolaore B, Mero A, Veronese FM (2008) Site-specific modification and PEGylation of pharmaceutical proteins mediated by transglutaminase. Adv Drug Deliv Rev 60:13–28

Fuchsbauer HL (2021) Approaching transglutaminase from *Streptomyces* bacteria over three decades. FEBS J 289:4680–4703

Ikura K, Nasu T, Yokota H, Tsuchiya Y, Sasaki R, Chiba H (1988) Amino acid sequence of guinea pig liver transglutaminase from its cDNA sequence. Biochemistry 27:2898–2905

Ishikawa K, Kimura S, Kanaya S, Morikawa K, Nakamura H (1993) Structural study of mutants of *Escherichia coli* ribonuclease HI with enhanced thermostability. Protein Eng 6:85–91

Kabsch W (1993) Automatic processing of rotation diffraction data from crystals of initially unknown symmetry and cell constants. J Appl Cryst 26:795–800

Kashiwagi T, Yokoyama K, Ishikawa K, Ono K, Ejima D, Matsui H, Suzuki E (2002) Crystal structure of microbial transglutaminase from *Streptoverticillium mobaraense*. J Biol Chem 277:44252–44260

Kikuchi Y, Date M, Yokoyama K, Umezawa Y, Matsui H (2003) Secretion of active-form *Streptoverticillium mobaraense* transglutaminase by *Corynebacterium glutamicum*: processing of the pro-transglutaminase by a cosecreted subtilisin-Like protease from *Streptomyces albogriseolus*. Appl Environ Microbiol 69:358–366

Mansfeld J, Vriend G, Dijkstra BW, Veltman OR, Van den Burg B, Venema G, Ulbrich-Hofmann R, Eijsink VG (1997) Extreme stabilization of a thermolysin-like protease by an engineered disulfide bond. J Biol Chem 272:11152–11156

Marx CK, Hertel TC, Pietzsch K (2008) Random mutagenesis of a recombinant microbial transglutaminase for the generation of thermostable and heat-sensitive variants. J Biotechnol 136:156–162

Matsumura M, Signor G, Matthews B (1989) Substantial increase of protein stability by multiple disulphide bonds. Nature 342:291–293

McPherson A, DeLucas L (2015) Microgravity Protein Crystallization. Npj Microgravity 1:15010

Murshudov GN, Vagin AA, Dodson EJ (1997) Refinement of macromolecular structures by the maximum-likelihood method. Acta Crystallogr D Biol Crystallogr 53:240–255

Nakamura A, Ohtsuka J, Miyazono K, Yamamura A, Kubota K, Hirose R, Hirota N, Ataka M, Sawano Y, Tanokura M (2012) Improvement in quality of protein crystals grown in a high magnetic field gradient. Cryst Growth Des 12:1141–1150

Navaza J (1994) AMoRe: an automated package for molecular replacement. Acta Crystallogr A 50:157–163

Nonaka M, Tanaka H, Okiyama A, Motoki M, Ando H, Umeda K, Matsuura A (1989) Polymerization of several proteins by calcium-independent transglutaminase derived from microorganisms. Agric Biol Chem 53:2619–2623

Oteng-Pabi SK, Keillor JW (2013) Continuous enzyme-coupled assay for microbial transglutaminase activity. Anal Biochem 441:169–173

Pace CN, Grimsley GR, Thomson JA, Barnett BJ (1988) Conformational stability and activity of ribonuclease T1 with zero, one, and two intact disulfide bonds. J Biol Chem 263:11820–11825

Pasternack R, Dorsch S, Otterbach JT, Robenek IR, Wolf S, Fuchsbauer HL (1998) Bacterial pro-transglutaminase from *Streptoverticillium mobaraense*: purification, characterization and sequence of zymogen. Eur J Biochem 257:570–576

Sambrook J, Fritsch EF, Maniatis T (1989) Molecular cloning: a laboratory manual, 2nd edn. Cold Spring Harbor Laboratory, Cold Spring Harbor, New York

Shimba N, Yokoyama K, Suzuki E (2002) NMR-based screening method for transglutaminases: rapid analysis of their substrate specificities and reaction rates. J Agric Food Chem 50:1330–1334

Suzuki M, Date M, Kashiwagi T, Suzuki E, Yokoyama K (2022) Rational design of a disulfide bridge increases the thermostability of microbial transglutaminase. Appl Microbial Biotechnol 106:4553–4562

Wang X, Du Jianhui J, Zhao B, Wang H, Rao S, Du G, Zhou J, Chen J, Liu S (2021) Significantly Improving the Thermostability and Catalytic Efficiency of *Streptomyces mobaraenesis* Transglutaminase through Combined Rational Design. J Agric Food Chem 69:15268–15278

Winn MD, Ballard CC, Cowtan KD, Dodson EJ, Emsley P, Evans PR, Keegan RM, Krissinel EB, Leslie AGW, McCoy A, McNicholas SJ, Murshudov GN, Pannu NS, Potterton EA, Powell HR, Read RJ, Vagin A, Wilson KS (2011) Overview of the CCP4 suite and current developments. Acta Crystallogr D Biol Crystallogr 67:235–242

Yang P, Wang X, Ye J, Rao S, Zhou J, Du G, Liu S (2023) Enhanced Thermostability and Catalytic Activity of *Streptomyces mobaraenesis* Transglutaminase by Rational Engineering Its Flexible Regions. J Agric Food Chem 71:6366–6375

Yokoyama K, Utsumi H, Nakamura T, Ogaya D, Shimba N, Suzuki E, Taguchi S (2010) Screening for improved activity of a transglutaminase from *Streptomyces mobaraensis* created by a novel rational mutagenesis and random mutagenesis. Appl Microbial Biotechnol 87:2087–2096

Yokoyama K, Ogaya D, Utsumi H, Suzuki M, Kashiwagi T, Suzuki E, Taguchi S (2021) Effect of introducing a disulfide bridge on the thermostability of microbial transglutaminase from *Streptomyces mobaraensis*. Appl Microbial Biotechnol 105:2737–2745

Zhu Y, Tramper J (2008) Novel applications for microbial transglutaminase beyond food processing. Trends Biotechnol 26:559–565